Pergamon

PII: S0022-4073(98)00012-0

J. Quant. Spectrosc. Radiat. Transfer Vol. 60, No. 3, pp. 365–374, 1998

Printed in Great Britain
0022–4073/98 $19.00 + 0.00

MICROWAVE RADIATIVE TRANSFER WITH NONSPHERICAL PRECIPITATING HYDROMETEORS

HARALD CZEKALA† and CLEMENS SIMMER

Meteorological Institute at the University of Bonn, Auf dem Hügel 20, 53121 Bonn, Germany

Abstract—We present the results of radiative transfer calculations in the microwave region focussing on the effects of multiple scattering by non-spherical hydrometeors. The use of microwave frequencies, e.g. 37 GHz, leads to a size parameter of 1.5 for raindrops with 4 mm diameter and requires an exact scattering solution rather than Rayleigh approximation. The distortion of raindrop shapes from the spherical geometry becomes significant and has to be taken into account when the scattering properties are calculated. The model developed uses the full Stokes vector to include the effects of cross-polarization terms between all Stokes components, which are important when the scattering of non-spherical particles is considered. The one-dimensional microwave radiative transfer model is based on the successive order of scattering method and assumes azimuthal symmetry. The shape of the hydrometeors is approximated by rotational symmetric ellipsoids with a size dependent aspect ratio. These particles have a fixed orientation with their rotational axis aligned along the vertical. Results for non-spherical and spherical scattering are presented. The differences between both methods, leading to 15 K change in the polarization difference depending on rain rate, frequency and viewing angle, are discussed.

1. INTRODUCTION

Microwaves are best suited and widely used for remote sensing of precipitation, e.g. with the frequencies of 19.35, 22.235, 37.0 and 85.5 GHz that are deployed on the Special Sensor Microwave/Imager (SSM/I) which is operated on satellites from the Defence Meteorological Satellite Project (DMSP). Measurements from this sensor in a polar, sun synchronous orbit in 833 km height are widely used for estimation of rainfall.[1–4]

The microwave radiation emerging from a cloud is determined by the temperature, size distribution, phase and shape of the hydrometeors. Up to now most microwave radiative transfer models apply Lorenz–Mie theory to calculate the effect of scattering and therefore assume spherical geometry for all hydrometeors. This is a poor approximation when focussing on falling raindrops which influence the microwave signal of the atmosphere strongly. These drop shapes can be described by a series of Chebyshev polynoms as given by Chuang and Beard.[5]

The scattering behaviour of these non-spherical particles can not be calculated with analytical theories and therefore requires numerical approaches. In the regime of sufficiently large size parameters, which is defined by $\chi = 2\pi r/\lambda$ and gives the ratio of particle size compared to wavelength, the geometrical optics approximation is used to investigate the scattering behaviour of raindrops and possible applications for remote sensing of rain rates with lidar techniques.[6] At smaller size parameters the geometrical optics approximation is no longer valid and the Lorenz–Mie theory for perfect spheres must be replaced by single scattering models which take into account the deformation of the target. The non-sphericity, combined with the preferred particle orientation, leads to changes in the radiative transfer equation and the interaction parameters, which are the extinction matrix, the scattering matrix and the emission vector. Theoretical studies concerning the attenuation of electromagnetic waves by non-spherical particles have been carried out by Oguchi[7,8]

† To whom all correspondence should be addressed.

and also by Asano and Yamamoto[9] more than 20 years ago. However, even recent studies by Li et al[10] do not include the full scattering phase function and angle dependent extinction coefficients. An application to the real atmosphere and microwave radiative transfer was the approach of Wu and Weinman, who used different extinction coefficients for vertical and horizontal polarization.[11] Again, these coefficients are still orientational averages. Evans and Stephens[12,13] carried out a study with realistically shaped ice crystal that were aligned to the horizontal with their longest dimension and randomly oriented in azimuthal directions. Their main objective was the investigation of brightness temperature depression in two specific directions and the sensitivity to the ice water content of cirrus cloud. To our knowledge that is the first study of microwave radiative transfer that uses angular dependent interaction parameters for nonspherical raindrops and gives a discussion on the angular dependence of the calculated brightness temperatures.

The following section describes the shape of falling water drops. In Sec. 3 the theory of polarized microwave radiative transfer is reviewed. The models we use in this study, both radiative transfer and single scattering, are described in Sec. 4. The results of our numerical calculations are presented in Sec. 5 with a discussion of the observed effects. Sec. 6 summarizes our conclusions.

2. DROP SHAPE

The shape of falling drops depends on terminal velocity and size. It can be computed by sophisticated models taking into account internal and external pressure, surface tension, friction of air and electric fields.[14,15] Larger drops reach higher terminal velocities and are therefore more distorted from the spherical geometry which seems to be a good approximation for smaller drops with a diameter well below 1 mm.

The resulting equilibrium shape of the axis-symmetric drop is expanded in a series of Chebyshev polynomials $\cos(n\theta)$ so that the radius $r(\theta)$ with respect to the zenith ange θ is given by

$$r(\theta) = r_0\left(1 + \sum_{n=0}^{N} c_n \cos(n\theta)\right). \tag{1}$$

The radius of the undistorted drop is given by r_0, the coefficients c_n ($n = 0, 1, \ldots, 10$) for drop sizes from 1 to 9 mm diameter are taken from Chuang and Beard.[5] The resulting drop shape cross sections are shown in Fig. 1. Significant flattening of the drop occurs at diameters above 3 mm. A commonly used parameter for the description of the drop deformation is the aspect ratio, defined as the ratio of the maximum horizontal size to the maximum vertical size of the drop.

Chuang and Beard give a parametrization of the aspect ratio α in form of a fourth order polynomial of the radius r as follows (Fig. 2):

$$\alpha = 1.01668 - 0.98055r - 2.52686r^2 + 3.75061r^3 + 1.68692r^4. \tag{2}$$

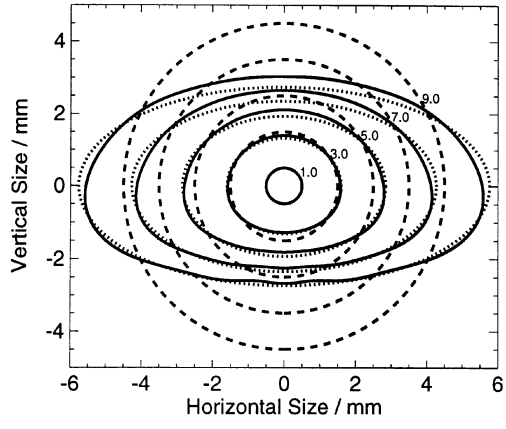

Fig. 1. Dropshape depending on dropsize: The numbers on the plotted shape give the diameter of the undisturbed spherical drop with equivalent volume (dashed lines). The dotted lines give the shape of the equivalent spheroid.

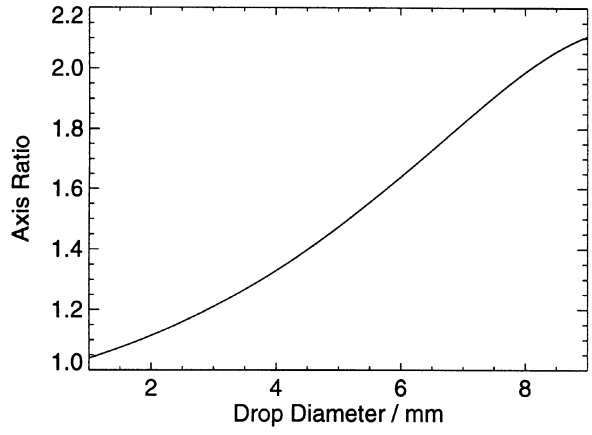

Fig. 2. Aspect ratio α as a function of drop diameter according to parametrization (2).

A further simplification can be done by limiting the shapes to rotational symmetric ellipsoids (also called spheroids), which is necessary because of geometric restrictions in the single scattering model that is used for this study: The shapes need to be symmetric to both, the axis and the plane of rotation. In this case the equivalent volume is represented by an spheroid with a minor and major axis defined by the aspect ratio α of parametrization (2).

3. RADIATIVE TRANSFER THEORY

Even if only the total intensity is of interest we have to use the polarized Stokes vector $\bar{\boldsymbol{I}} = (I_v, I_h, U, V)$ when calculating radiative transfer with non-spherical particles.[16] Furthermore, the Stokes vector provides additional information about polarization, which is strongly affected by the shape of hydrometeors. From the electric field components of a polarized wave, E_l and E_r, the Stokes vector can be defined as

$$\bar{\boldsymbol{I}} = \begin{pmatrix} I_v \\ I_h \\ U \\ V \end{pmatrix} = \begin{pmatrix} |E_v|^2 \\ |E_h|^2 \\ 2\,\mathrm{Re}(E_v E_h^*) \\ 2\,\mathrm{Im}(E_v E_h^*) \end{pmatrix}. \tag{3}$$

3.1. Vector radiative transfer equation

If we consider anisotropic media we have to define the interaction parameters, such as extinction, emission and scattering, with respect to the direction of incoming radiation.[12,13] The differential change of the radiation intensity described by the Stokes vector, at height z and direction (θ, ϕ), is given by the vector radiative transfer equation (4). The equation describes the intensity loss (extinction) due to scattering and absorption, the radiation source that comes from thermal emission obeying Planck's law $B(T)$, and the scattering source term. The last contribution redirects radiation from all incident directions (θ', ϕ') to the specific direction (θ, ϕ). This process is fully described by the scattering phase matrix $\boldsymbol{P}$.

$$\cos\theta \frac{\mathrm{d}\bar{\boldsymbol{I}}(z,\theta,\phi)}{\mathrm{d}z} = -\overbrace{\bar{\bar{\sigma}}_e(z,\theta,\phi)}^{\text{extinction matrix}}\bar{\boldsymbol{I}}(z,\theta,\phi) + \overbrace{\bar{\sigma}_a(z,\theta,\phi)\,B(T(z))}^{\text{emission vector}} + \int_0^{2\pi}\int_0^{\pi} \underbrace{\bar{\bar{\boldsymbol{P}}}(z,\theta,\phi;\ \theta',\phi')}_{\text{phase matrix}}\bar{\boldsymbol{I}}(z,\theta',\phi')\sin\theta'\,\mathrm{d}\theta'\,\mathrm{d}\phi'. \tag{4}$$

All interaction parameters depend on the atmospheric conditions at height z and the direction, which is given by the zenith and azimuth angles θ and ϕ, respectively.

3.2. Calculation of interaction parameters with the amplitude scattering function

Single scattering of a polarized electromagnetic plane wave (given by the components E_{vi} and E_{hi} of the electric field) can be described with the complex amplitude scattering function $f_{rt}(r, t = v, h)$. This is a 2×2 matrix with four complex elements that couples the scattered electric field E_{vs} and E_{hs} with the incident field:

$$\begin{pmatrix} E_{vs}(\theta, \phi) \\ E_{hs}(\theta, \phi) \end{pmatrix} = \begin{pmatrix} f_{vv}(\theta, \phi; \theta', \phi') & f_{vh}(\theta, \phi; \theta', \phi') \\ f_{hv}(\theta, \phi; \theta', \phi') & f_{hh}(\theta, \phi; \theta', \phi') \end{pmatrix} \begin{pmatrix} E_{vi}(\theta', \phi') \\ E_{hi}(\theta', \phi') \end{pmatrix}. \tag{5}$$

This matrix can be calculated by single scattering models (see Sec. 4.2). When Lorenz–Mie scattering is used the amplitude scattering matrix is diagonal due to the spherical geometry of the target. The nondiagonal form of this matrix in the non-spherical case leads to a more complex behaviour and makes the application of a full extinction matrix and an emission vector necessary.

The interaction parameters can be calculated applying equation (5) using the Stokes vector definition (3).[16] The extinction matrix $\bar{\bar{\sigma}}_e(\theta, \phi)$ is computed with the optical theorem from the forward scattering amplitudes. With equal angles $\theta = \theta'$, $\phi = \phi'$ and the definition $M_{jl} = (i2\pi/k) f_{jl}(\theta, \phi; \theta, \phi)$ it reads:

$$\bar{\bar{\sigma}}_e(\theta, \phi) = \begin{pmatrix} -2\,\mathrm{Re}(M_{vv}) & 0 & -\mathrm{Re}(M_{vh}) & -\mathrm{Im}(M_{vh}) \\ 0 & -2\,\mathrm{Re}(M_{hh}) & -\mathrm{Re}(M_{hv}) & \mathrm{Im}(M_{hv}) \\ -2\,\mathrm{Re}(M_{hv}) & -2\,\mathrm{Re}(M_{vh}) & -(\mathrm{Re}(M_{vv}) + \mathrm{Re}(M_{hh})) & (\mathrm{Im}(M_{vv}) - \mathrm{Im}(M_{hh})) \\ 2\,\mathrm{Im}(M_{hv}) & -2\,\mathrm{Im}(M_{vh}) & -(\mathrm{Im}(M_{vv}) - \mathrm{Im}(M_{hh})) & -(\mathrm{Re}(M_{vv}) + \mathrm{Re}(M_{hh})) \end{pmatrix}. \tag{6}$$

All four angles are necessary for the scattering phase matrix $\bar{\bar{\boldsymbol{P}}}(\theta, \phi; \theta', \phi')$:

$$\bar{\bar{\boldsymbol{P}}}(\theta, \phi; \theta', \phi') = \begin{pmatrix} |f_{vv}|^2 & |f_{vh}|^2 & \mathrm{Re}(f_{vh}^* f_{vv}) & -\mathrm{Im}(f_{vh}^* f_{vv}^*) \\ |f_{hv}|^2 & |f_{hh}|^2 & \mathrm{Re}(f_{hh}^* f_{hv}) & -\mathrm{Im}(f_{hv} f_{hh}^*) \\ 2\,\mathrm{Re}(f_{vv} f_{hv}^*) & 2\,\mathrm{Re}(f_{vh} f_{hh}^*) & \mathrm{Re}(f_{vv} f_{hh}^* + f_{vh} f_{hv}^*) & -\mathrm{Im}(f_{vv} f_{hh}^* - f_{vh} f_{hv}^*) \\ 2\,\mathrm{Im}(f_{vv} f_{hv}^*) & 2\,\mathrm{Im}(f_{vh} f_{hh}^*) & \mathrm{Im}(f_{vv} f_{hh}^* + f_{vh} f_{hv}^*) & \mathrm{Re}(f_{vv} f_{hh}^* - f_{vh} f_{hv}^*) \end{pmatrix}. \tag{7}$$

The absorption in the case of non-spherical particles is no longer a single number but becomes a four component vector that varies with the direction of incidence. Generally, it is the total radiation loss (extinction) minus all radiation which is scattered into other directions than the direction of propagation. We obtain

$$\bar{\sigma}_a(\hat{r}) = \begin{pmatrix} \frac{4\pi}{k}\,\mathrm{Im}\, f_{vv}(\hat{r}, \hat{r}) - \int \mathrm{d}\Omega' (|f_{vv}(\hat{r}', \hat{r})|^2 + |f_{hv}(\hat{r}', \hat{r})|^2) \\ \frac{4\pi}{k}\,\mathrm{Im}\, f_{hh}(\hat{r}, \hat{r}) - \int \mathrm{d}\Omega' (|f_{vh}(\hat{r}', \hat{r})|^2 + |f_{hh}(\hat{r}', \hat{r})|^2) \\ 2\,\mathrm{Re}\left\{ \frac{2\pi i}{k} [f_{vh}^*(\hat{r}, \hat{r}) - f_{hv}(\hat{r}, \hat{r})] - \int \mathrm{d}\Omega' [f_{vv}(\hat{r}', \hat{r})\, f_{vh}^*(\hat{r}', \hat{r}) + f_{hv}(\hat{r}', \hat{r}) f_{hh}^*(\hat{r}', \hat{r})] \right\} \\ 2\,\mathrm{Im}\left\{ \frac{2\pi i}{k} [f_{vh}^*(\hat{r}, \hat{r}) - f_{hv}(\hat{r}, \hat{r})] - \int \mathrm{d}\Omega' [f_{vv}(\hat{r}', \hat{r}) f_{vh}^*(\hat{r}', \hat{r}) + f_{hv}(\hat{r}', \hat{r})\, f_{hh}^*(\hat{r}', \hat{r})] \right\} \end{pmatrix}. \tag{8}$$

These quantities are correct for scattering by a single particle of a certain size. In order to calculate the radiation interaction parameters of a specific atmospheric layer we have to integrate equations (6)–(8) over particle size distributions. A widely used and very simple distribution with an

exponential increase in drop number for smaller drops is the Marshall–Palmer[17] distribution

$$n(r) = N_0 \exp(-qr) \tag{9}$$

with $N_0 = 16\,000\ \mathrm{m}^{-3}\ \mathrm{mm}^{-1}$, $q = 8.2\mathrm{RR}^{-0.21}$ and the rain rate RR given in mm h^{-1}.

4. MODEL

4.1. Radiative transfer model

The vector radiative transfer equation (4) is solved with a one-dimensional numerical model,[18] which considers the atmosphere as horizontally homogeneous with horizontally infinite plane parallel layers. At each layer the atmospheric conditions such as temperature, pressure, humidity, cloud water content, cloud ice content, rain rate for liquid and frozen hydrometeors have to be known.

The radiation interaction parameters are computed for each layer. The gas absorption coefficients due to water vapour, molecular oxygen and nitrogen are calculated using the Millimeter Propagation Model (MPM) code from Liebe.[19,20] Absorption, extinction, and scattering by hydrometeors are calculated with the single scattering models described in the following subsection. The azimuth dependency is eliminated through integration. The resulting scattering, extinction and absorption parameters only depend on zenith angles.

The radiation and all interaction parameters are calculated at a set of arbitrary discrete zenith angles. The polarization state of the radiation is represented by the four component Stokes vector as defined in Eq. (3). The radiative transfer equation is solved by the successive order of scattering method.

The boundary conditions at the top and the bottom of the atmosphere are set to cosmic background temperature and the land surface temperature, respectively. Surface emission is considered to be independent of frequency and direction, therefore only the emissivity determines the lower boundary condition. In the calculations shown later the emissivity is set to either $\varepsilon = 0.0$ or $\varepsilon = 1.0$. Land surfaces have typical values of $\varepsilon = 0.9$ and therefore show a strong radiation emission in the upward directions. The situation with $\varepsilon = 0.0$ gives the opportunity to study effects of atmospheric radiation without the dominant surface emission.

4.2. Single scattering model

The size of scattering particles is close to the wavelength of microwave frequencies if raindrops and ice particles are considered. A drop of 4 mm diameter, for example, leads at a frequency of 37 GHz to a size parameter of 1.5. The situation becomes worse at 183 GHz where a small droplet of 200 μm diameter produces a size parameter of 0.38. In these cases the Rayleigh approximation fails and an exact solution must be used. The Lorenz–Mie theory is exact for particles of any size, but only valid for spheres.

Due to their non-spherical shape raindrops and ice particles need numerical scattering models for exact calculations. Among various T-Matrix methods the Extended Boundary Condition Method (EBCM) is a very effective and precise method. A detailed description of the T-Matrix approach can be found in a review from Mishchenko et al[21] and the references therein. We use a EBCM code from Michael Mishchenko which is available to public domain.[22] Input parameters are wavelength, refractive index, particle size and particle shape. The possible particle shapes are restricted to rotational symmetric objects having an additional plane of symmetry perpendicular to the rotation axis. After computing the T-Matrix once for every particle the program calculates the amplitude scattering function at a set of discrete incident and scattered directions. In this calculations the natural coordinate system of the particle is used where the z-axis is aligned to the axis of particle symmetry.

Due to the limitations in particle shape we have approximated the realistic drop shapes of Eq. (1) with oblate spheroids of the same volume, both shown in Fig. 1. The aspect ratio of the spheroids depends on size and is taken from the parametrization (2).

5. RESULTS AND DISCUSSION

The polarized radiative transfer model was used to calculate microwave brightness temperatures for some typical frequencies. All calculations are carried out both for spheres and oblate spheroids.

The effect of non-sphericity is shown as the difference between the results with oblate drops and the results with perfect spheres as calculated with the Lorenz–Mie theory.

5.1. *Angle dependent brightness temperatures*

Realistic atmospheric conditions for a raining midlatitude summer day were used in these calculations. In the lowest 4000 m of the atmosphere a raining cloud with a rain rate of up to 58 mm h^{-1} is positioned. The rain rate reaches its maximum at the bottom of the cloud, having smaller rain rates above and below. The liquid water path of the cloud is 1.1 kg m^{-2}, the integrated rain is about 7.6 kg m^{-2}. The surface temperature is set to 290 K and an emissivity of $\varepsilon = 1.0$. In this calculations 8 Gaussian angles per hemisphere are used. In Fig. 3 brightness temperatures are plotted for 8 upward directions at the top of the atmosphere and 8 downward directions at the bottom of the atmosphere, respectively. All calculations are shown at three frequencies: 10.7, 19.35, and 37.0 GHz.

The upper three graphs of Fig. 3 shows the total intensity, the lower three graphs the polarization difference. Calculations with rain drops considered as perfect spheres are in the left column, followed by calculations with oblate drops with a size dependent aspect ratio. In the third column the difference of both calculations is given.

The total intensities show very similar patterns in the spherical and non-spherical case: Upward directed radiation represents the temperature of the surface and, as the optical thickness increases with frequency, the temperature of the upper atmosphere. Downward directed radiation mainly consists of the temperature signal from the lowest rain layers and in case of the lower frequencies the cold radiation from space.

Stronger differences can be observed in the polarization difference ($I_v - I_h$): In both cases the upward radiation shows a positive polarization difference which increases with viewing angle. In case of the non-spherical calculations the effect is significantly stronger. Rather interesting are the polarization signals in directions pointing down to the surface. For those frequencies with the lowest optical thickness a strong negative polarization difference of up to -10 K occurs. We believe that this is an effect of the predominantly upward directed radiation field: Only the atmospheric emission is nearly isotropic, the surface emission produces an additional amount of radiation that is only directed to the top of the atmosphere. This leads to an angle dependent background radiation field, which is known to produce polarization effects even in the case of Lorenz–Mie scattering.[22]

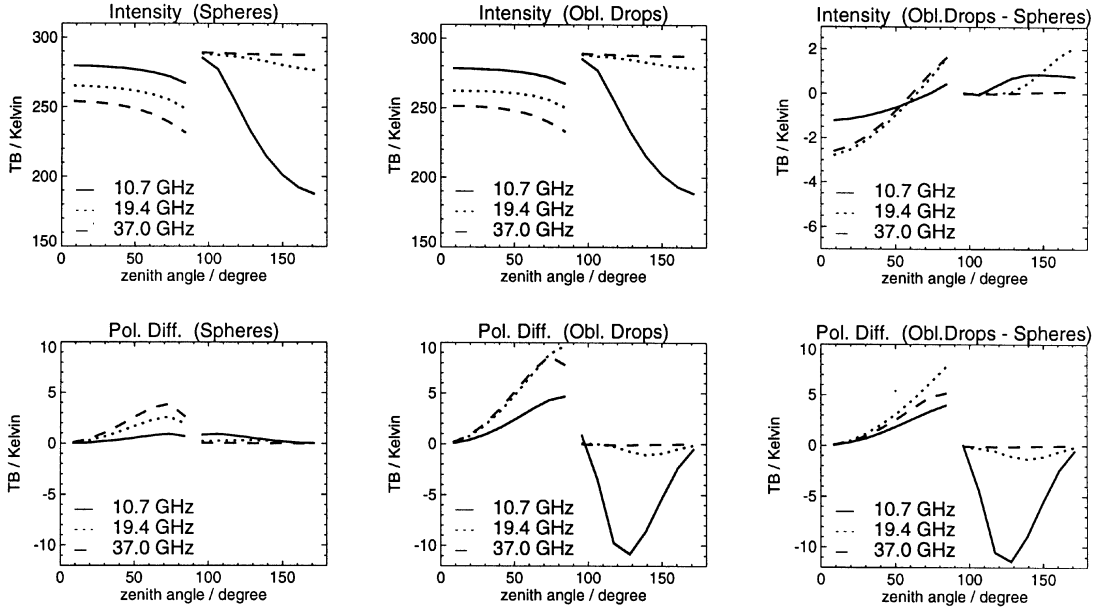

Fig. 3. Brightness temperatures and polarization differences versus zenith angle in a raining atmosphere with emissivity $\varepsilon = 1.0$ at bottom (for details see text). Upward direction is at zero angle, downward at 180°.

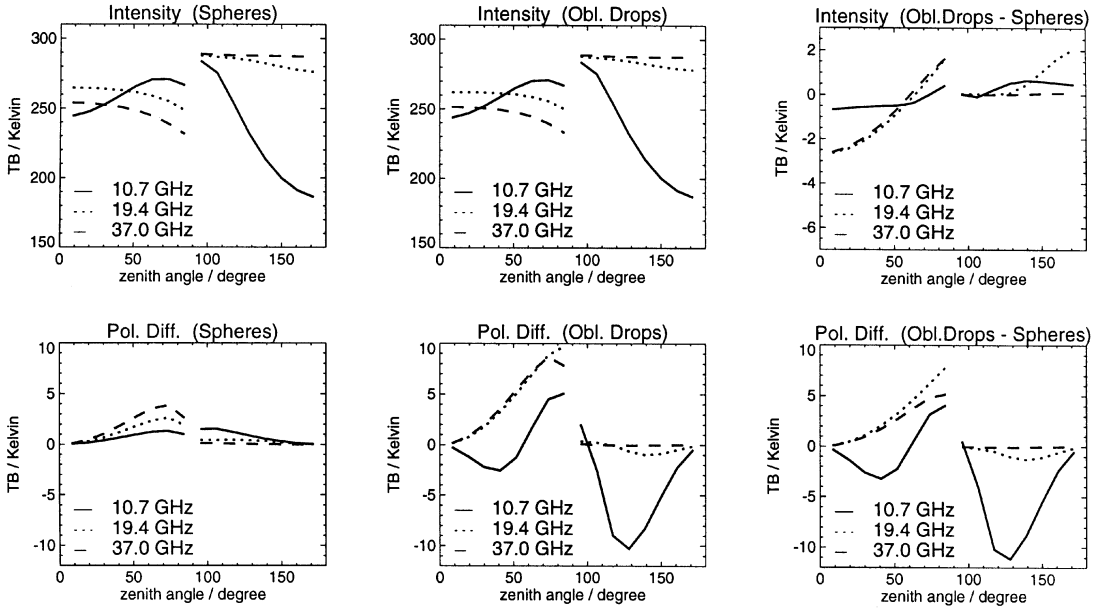

Fig. 4. Brightness temperatures and polarization differences versus zenith angle in a raining atmosphere with emissivity $\varepsilon = 0.0$. All other parameters as in Fig. 3.

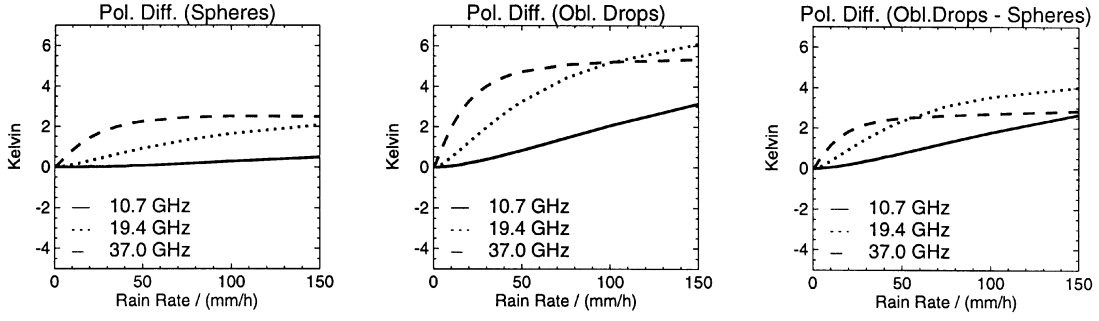

Fig. 5. Polarization differences versus rain rate at a viewing angle $\theta = 51.8°$.

Changing surface emissivity to zero (obtaining a reflectivity of 1.0), but leaving all other parameters unchanged, we reduce the radiation within the atmosphere to the atmospheric thermal emission only. The results are shown in Fig. 4. Now negative polarization differences occur also in upward directions, but only at 10.7 GHz. This behaviour is frequency dependent due to the variation of optical thickness with frequency. When the atmosphere becomes opaque there is a nearly isotropic radiation field whereas the low frequencies penetrate deep into the atmosphere and "sense" the different temperatures at different levels.

5.2. Sensitivity to rainfall

The effect of different rain rates on the calculated brightness temperatures is studied with simplified atmospheric conditions. Only one model layer at the bottom of the atmosphere is filled with rain with a vertically constant rain rate. The surface emissivity is set to 1.0, all other parameters are the same as in the previous calculations.

Due to minor differences in total intensity between the spherical and non-spherical calculations we only present polarization differences. In Fig. 5 we can see the different behaviour of oblate spheroids in radiative transfer in a direction of $\theta = 51.8°$ which is close to the viewing angle of

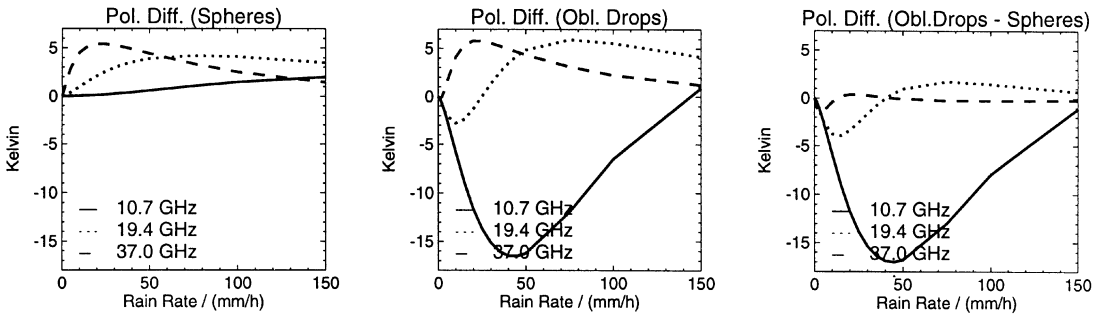

Fig. 6. Polarization differences versus rain rate at a viewing angle of $\theta = 95.5^\circ$.

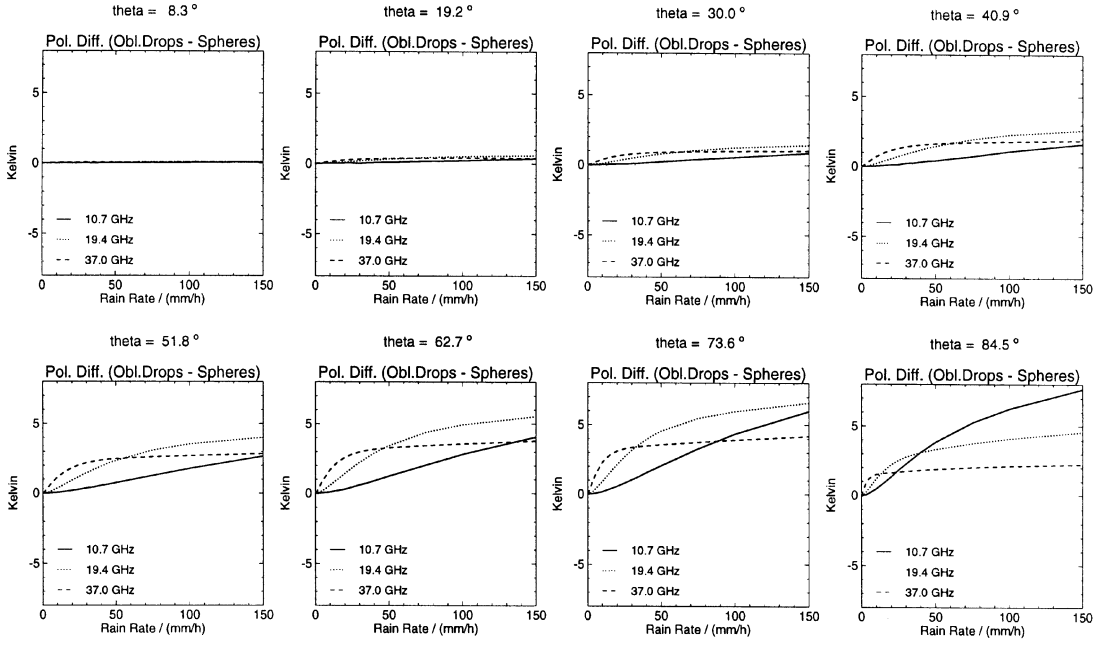

Fig. 7. Difference of polarization differences (non-spherical minus spherical) versus rain rate at upward directions.

SSM/I. The polarization signal tends to increase with higher rain rates in both cases, but the non-spherical result is much stronger at every given rain rate.

A more complex situation is obtained for ground observations of radiation in downward directions (Fig. 6). Here we selected an extreme case ($\theta = 95.5^\circ$) of observation close to the horizontal. With Lorenz–Mie scattering the polarization difference decreases after a first peak at low rain rates. The position of this peak is frequency dependent (at lower rain rates for higher frequencies). Non-spherical calculations show a negative peak in front of the positive peak, especially at low frequencies. With increasing frequencies this negative polarization difference signal gets weaker and at 37 GHz there is nearly no difference between spherical and non-spherical calculations.

The described effects in the polarization difference are strongly dependent on the viewing angle. Figure 7 shows the difference of non-spherical and spherical calculations at eight upward directions. The same quantities for the downward directions are shown in Fig. 8. Close to 0 and 180° no polarization difference can be observed due to the definition of horizontal and vertical polarization. Varying the angle from zero to $\approx 55^\circ$ increases the non-spherical signal, strongest for the higher frequencies. If the direction of radiation gets closer to the horizontal the optical path gets longer and

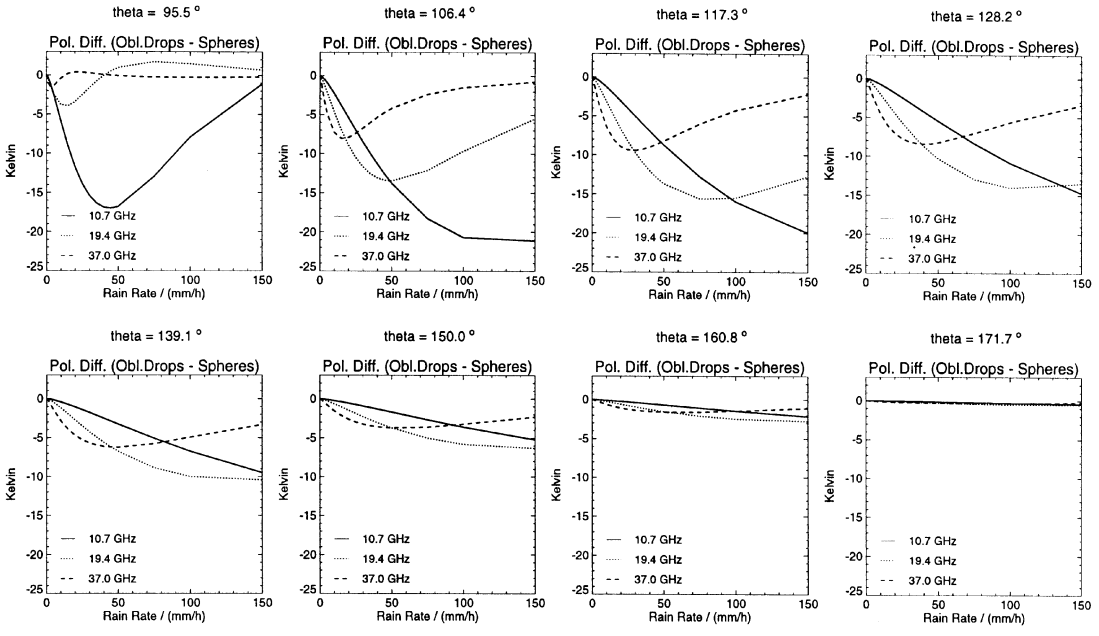

Fig. 8. Difference of polarization differences (non-spherical minus spherical) versus rain rate at downward directions.

the total optical thickness is increased. In this situation the high frequencies begin to saturate whereas the low frequency (10.7 GHz) still has the ability to penetrate the atmosphere, leading to a further increase in polarization difference.

Generally negative polarization differences result for downward directions. Again, this behaviour is strongest close to the horizontal. The signal increases to higher rain rates, but diminishes to zero when a certain optical thickness is reached. The total optical thickness depends on rain rate, viewing angle, and the frequency under consideration. With $\theta = 106.4^\circ$ and $\theta = 95.5^\circ$ the optical path is dramatically increased so that saturation begins at lower rain rates. Then the polarization difference rises again after the first negative peak and even positive values can be reached, e.g. for 19.35 GHz at $\theta = 95.5^\circ$.

6. SUMMARY AND CONCLUSIONS

We developed a radiative transfer model that takes into account the non-spherical geometry of hydrometeors in the atmosphere. Single scattering properties are calculated with the amplitude scattering function computed using the T-Matrix method. The realistic drop shapes, expressed in a series of Chebyshev polynoms, were approximated by rotational symmetric ellipsoids (spheroids) with same aspect ratio and equal volume.

The influence of the spheroid shape on microwave brightness temperatures is calculated. We show that in the case of intense rain the radiative transfer gives significant changes. The total intensity of brightness temperature is less affected than the polarization difference. Angular distributions of the polarization differences depend on the direction and intensity of the radiation in the atmosphere on which the surface emissivity has a strong impact.

Calculations with different rain rates state that the effect of raindrop shape also depends on the total amount of rain and leads to higher positive polarization differences for all upward directions. Radiation pointing to the surface produces a negative polarization difference with a more complex dependency from rain rate, frequency, and viewing angle.

Acknowledgements—We wish to thank Michael Mishchenko for making available the EBCM code and also for helpful comments while merging this code into the radiative transfer model. This work was supported by the Deutsche Forschungsgemeinschaft under Si 606/1–1.

REFERENCES

1. Adler, R. F., Negri, A. J., Keen, P. and Hakkarinen, I. M., Estimation of monthly rainfall over Japan and surrounding waters from a combination of low-orbit microwave and geosynchronous IR data. *J. Appl. Meteorol*., 1993, **32,** 335–356.
2. Bauer, P. and Grody, N., The potential of combining SSM/I and SSM/T2 measurements to improve the identification of snowcover and precipitation. *IEEE Trans. on Geoscience and Remote Sensing*, 1995, **33,** 252–261.
3. Petty, G. W. and Katsaros, K. B., Precipitation observed over the south china sea by the Nimbus-7 scanning multichannel microwave radiometer during winter monex. *J. Appl. Meteorol*., 1990, **29,** 273–287.
4. Prabhakara, C., Dalu, G., J. J. Nucciarone, R. S. and Liberti, G. L. Rainfall over oceans: Remote sensing from satellite microwave radiometers. *Meteorol. Atmos. Phys*., 1992, **47,** 177–199.
5. Chuang, C. and Beard, K. V., A numerical model for the equilibrium shape of electrified raindrop. *J. Atmos. Sci*., 1990, **47**(11)**,** 1374–1389.
6. Macke, A. and Grossklaus, M., Light scattering at nonspherical raindrops: Possible applications for remote sensing of rainrates. *JQSRT*, 1998, (submitted).
7. Oguchi, T., Attenuation of electromagnetic wave due to rain with distorted raindrops. *J. Radio Res. Laboratories*, 1960, **7**(33)**,** 467–485.
8. Oguchi, T., Attenuation of electromagnetic wave due to rain with distorted raindrops (Part II). *J. Radio Res. Laboratories*, 1964, **11**(53)**,** 19–44.
9. Asano, S. and Yamamoto, G., Light scattering by a spheroidal particle. *Appl. Opt*., 1975, **14,** 29–49.
10. Li, L. -W., Kooi, P. -S., Leong, M. -S., Yeo, T. -S. and Gao, M. -Z., Microwave attenuation by realistically distorted raindrops: Part II — predictions. *IEEE Trans. on Antennas and Propagation*, 1995, **43**(8)**,** 823–828.
11. Wu, R. and Weinman, J. A., Microwave radiances from precipitating clouds containing aspherical ice, combined phase, and liquid hydrometeors. *J. Geophys. Res*., 1984, **89,** 7170–7178.
12. Evans, K. F. and Stephens, G. L., Microwave radiative transfer through clouds composed of realistically shaped ice crystals Part I: Single scattering properties. *J. Atmos. Sci*., 1995a, **52**(11)**,** 2041–2057.
13. Evans, K. F. and Stephens, G. L., Microwave radiative transfer through clouds composed of realistically shaped ice crystals Part II: Remote sensing of ice clouds. *J. Atmos. Sci*., 1995b, **52**(11)**,** 2058–2072.
14. Beard, K. V. and Chuang, C., A new model for the equilibrium shape of raindrops. *J. Atmos. Sci*., 1987, **44,** 1509–1524.
15. Feng, J. Q. and Beard, K. V., A perturbation model of raindrop oscillation characteristics with aerodynamic effects. *J. Atmos. Sci*., 1991, **48**(16)**,** 1856–1868.
16. Tsang, L., Kong, J. A. and Shin, R. T., *Theory of Microwave Remote Sensing*. Wiley, New York, 1985, 613p.
17. Marshall, J. S. and Palmer, M., The distribution of raindrops with size. *J. Meteorol*., 1948, **5,** 165–166.
18. Simmer, C., *Satellitenfernerkundung hydrologischer Parameter der Atmosphäre mit Mikrowellen*. Verlag Dr. Kovac, Hamburg, 1994, 314p.
19. Liebe, H. J., An updated model for millimeter wave propagation in moist air. *Radio Sci*., 1985, **20,** 1069–1089.
20. Liebe, H. J., Hufford, G. A. and Cotton, M. G., Propagation modeling of moist air and suspended water/ice particles at frequencies below 1000 GHz. In *AGARD* 52*nd Specialists Meeting of the Electromagnetic Wave Propagation Panel*, *Palma de Mallorca*, *Spain*, 1993.
21. Mishchenko, M. I., Travis, L. D., and Mackowski, D. W., T-matrix computations of light scattering by nonspherical particles: a review. *JQSRT*, 1996, **55**(5)**,** 535–575.
22. Mishchenko, M. I. and Travis, L. D., Light scattering by polydisperse, rotationally symmetric nonspherical particles: linear polarisation. *JQSRT*, 1994, **51,** 579–778.
23. Liu, Q. and Simmer, C., Polarisation and intensity in microwave radiative transfer. *Beiträge zur Physik der Atmosphäre*, 1996, **69,** 535–545.